universiteit hasselt

UHasselt Computational Mathematics Preprint Series

Klaus Kaiser and Jochen Schütz

A high-order method for weakly compressible flows

UHasselt Computational Mathematics Preprint Nr. UP-16-06

August 22, 2008

A high-order method for weakly compressible flows

Klaus Kaiser*,†, Jochen Schütz†

August 22, 2008

In this work, we introduce an IMEX discontinuous Galerkin solver for the weakly compressible isentropic Euler equations. The splitting needed for the IMEX temporal integration is based on the recently introduced *reference solution* splitting [1, 2], which makes use of the *incompressible* solution. We show that the resulting algorithm is *asymptotically consistent* (with the asymptotic being Mach number to zero) and *asymptotic preserving*, and we observe that it is *asymptotically stable* and *asymptotically accurate*. Furthermore, we give a systematic way of computing an approximate reference solution by considering the discrete limit method as a potential discretization. The final algorithm is shown to work well on a series of weakly-compressible test cases.

*IGPM, RWTH Aachen University, Templergraben 55, 52062 Aachen
†Faculty of Sciences, Hasselt University, Agoralaan Gebouw D, BE-3590 Diepenbeek

1. Introduction

In this work, we consider the (weakly-)compressible isentropic Euler equations [3, 4] in dimensionless form,

$$\begin{aligned} \rho_t + \nabla \cdot (\rho \boldsymbol{u}) &= 0 \\ (\rho \boldsymbol{u})_t + \nabla \cdot (\rho \boldsymbol{u} \otimes \boldsymbol{u}) + \frac{1}{\varepsilon^2} \nabla p &= 0. \end{aligned} \tag{1}$$

The wave speeds in normal direction $\boldsymbol{n}$ of this (assumed two-dimensional) problem are

$$\lambda_1 = \boldsymbol{u} \cdot \boldsymbol{n} \qquad \text{and} \qquad \lambda_{2,3} = \boldsymbol{u} \cdot \boldsymbol{n} \pm \frac{c}{\varepsilon}, \tag{2}$$

which means that there is a convective and two acoustic waves. In what follows, we assume that the reference Mach number ε is small, i.e., $\varepsilon \ll 1$, which physically means that the solution is a small disturbance of the incompressible solution. Indeed, it can be shown that under suitable requirements on initial and boundary data ("well-preparedness"), there is convergence of $(\rho, \rho\boldsymbol{u})$ towards its incompressible counterpart as $\varepsilon \to 0$, see [5, 6, 7]. Furthermore, it is obvious that this problem constitutes a *singularly perturbed equation* in ε, as the equations change type in the limit.

Due to the change of type as $\varepsilon \to 0$, the equations get extremely stiff and therefore it is highly non-trivial to design efficient and stable algorithms. Explicit-in-time solving techniques have the drawback that they lead to a CFL condition in which the time step size Δt must be proportional to (at least) $\varepsilon \Delta x$, where Δx is a measure for the spatial grid size. If it is not the goal to accurately resolve all the features, but only to resolve the convective part of the flow, this condition is extremely restrictive, and a so called *convective CFL condition*

$$\Delta t \lesssim \|\boldsymbol{u}\| \Delta x \tag{3}$$

is preferable. Fully implicit-in-time methods, on the other hand, which are stable under such a CFL condition, tend to add too much spurious diffusion [8].

In the past few years, so called IMEX splitting schemes got more and more popular for solving compressible flow problems, especially for low Mach numbers, see e.g. [9, 10, 11, 12, 13, 14, 15, 16, 17, 18] and the references therein. Optimally, such a scheme should be designed in a way that slow waves are handled with an explicit (thus efficient) and fast waves are handled with an implicit (thus stable) method. Of course such a strict splitting of waves is only possible in the linear one-dimensional case [19], and therefore, a suitable splitting for the nonlinear case has to be defined very carefully.

Over the past few years, many famous splittings for the Euler equations at low Mach number have been designed, beginning by the ground-breaking work of Klein [14]. For a non-exhaustive list, we refer to [9, 11, 13] and the references therein. However, many of those splittings have their shortcomings. It has been reported [20] that Klein's splitting seems to be unstable in some instances. (Which, however, does not include Klein's original algorithm, which is based on a semi discrete decoupling of the pressure.) Furthermore, all of the mentioned splittings need a physical intuition and are not directly extendable to other singularly perturbed differential equations.

To partly overcome these shortcomings, we have over the past few years developed a new type of splitting that is based on the $\varepsilon = 0$ ("incompressible") solution of the problem. The splitting, see Sec. 4, is generic in the sense that it can in principle be applied to any type of singularly perturbed equation, including singularly perturbed ODEs [1] and of course the Euler equations [2]. Related ideas have already been published earlier, for the shallow water equations in [9, 21] and for kinetic equations in [22], a stability analysis of the splitting has been done in [20] and [23].

In [1], we have applied the splitting idea to singularly perturbed ordinary differential equations with high-order IMEX discretizations, namely IMEX linear multistep methods [24, 25, 26] and IMEX Runge-Kutta methods [27, 28, 29, 30, 31, 32, 33]. In [2], we have applied the splitting idea to a low-order finite volume scheme for the isentropic Euler equation. In both publications, we have seen that the newly developed splitting can be highly advantageous. This present work is a 'natural' extension of those previous works: We combine a high-order-in-time IMEX Runge-Kutta scheme with a high-order-in-space discontinuous Galerkin (DG) method (see [34, 35, 36, 37, 38] for classical DG and [39, 40, 41] for IMEX DG) using the newly developed splitting. In this work, we show, partly analytically, partly numerically, that this particular IMEX DG method that we develop here fulfills the following properties:

- It is *asymptotically consistent* (AC), which means that its $\varepsilon \to 0$ limit is a consistent discretization of the corresponding incompressible equations. Furthermore, we numerically show that it is *asymptotic preserving*, which means that the limit algorithm is stable [42, 43, 44].

- It is *asymptotically stable* (AS), which means that the restriction on Δt does *not* depend on ε, but only on Δx, so we can work with a convective CFL condition (3).

- It is *asymptotically accurate* (AA), which means that the method delivers the desired convergence order independently of ε [45, 46].

In particular this last property is somewhat peculiar, because if it is not fulfilled, a high-order method is arguably useless for the $\varepsilon \ll 1$ case.

This paper is organized as follows: We introduce the equations and some examples in Sec. 2. The definitions concerning the asymptotic behavior are introduced in Sec. 3, followed by the presentation of the splitting in Sec. 4 and the fully discrete method in Sec. 5. Asymptotic properties of this method are analyzed in Sec. 6. As usually, the paper ultimately gives some conclusion and outlook in the last Sec. 7.

2. Governing equations and examples

In this section, we introduce the underlying equations, and we discuss some appropriate numerical examples.

2.1. Underlying equation

Let $\Omega \subset \mathbb{R}^2$ be a two-dimensional domain, and consider the isentropic Euler equations as in (1), with $\rho \in \mathbb{R}$ density and $\boldsymbol{u} = (u, v)^T \in \mathbb{R}^2$ velocity in $x-$ and $y-$direction, respectively. p denotes pressure given for polytropic fluids as $p(\rho) = \kappa\rho^\gamma$ with a $\kappa > 0$ and a $\gamma \geq 1$. Note that the reference Mach number ε is given by

$$\varepsilon := \frac{u^*}{\sqrt{p(\rho^*)/\rho^*}},$$

where u^* and ρ^* are the corresponding reference values for velocity and density, respectively. The isentropic Euler equations can directly be rewritten as a conservation law in divergence form

$$\boldsymbol{w}_t + \nabla \cdot \boldsymbol{f}^C(\boldsymbol{w}) = 0 \qquad \text{with} \qquad \boldsymbol{w} := \begin{pmatrix} \rho \\ \rho\boldsymbol{u} \end{pmatrix} \qquad \text{and} \qquad \boldsymbol{f}^C(\boldsymbol{w}) := \begin{pmatrix} \rho\boldsymbol{u} \\ \rho\boldsymbol{u} \otimes \boldsymbol{u} + \frac{1}{\varepsilon^2} p \cdot \mathrm{Id} \end{pmatrix}. \tag{4}$$

Id denotes the two dimensional identity matrix. Computing the eigenvalues of $\partial_{\boldsymbol{w}} \boldsymbol{f}^C \cdot \boldsymbol{n}$ gives the characteristic wave speeds

$$\lambda_1 = \boldsymbol{u} \cdot \boldsymbol{n} \qquad \text{and} \qquad \lambda_{2,3} = \boldsymbol{u} \cdot \boldsymbol{n} \pm \frac{c}{\varepsilon}, \tag{2}$$

where c denotes the speed of sound of the system. Obvisouly, these eigenvalues are on different scales w.r.t. ε. Scales can be best understood by considering an asymptotic expansion of every quantity, namely

$$\boldsymbol{w} = \boldsymbol{w}_{(0)} + \varepsilon \boldsymbol{w}_{(1)} + \varepsilon^2 \boldsymbol{w}_{(2)} + \mathcal{O}(\varepsilon^3). \tag{5}$$

Inserting this expansion into the isentropic Euler equations (1), collecting all terms in power of ε and taking the limit $\varepsilon \to 0$ formally leads to the incompressible Euler equations

$$\begin{aligned} \rho_{(0)} \equiv \text{const} > 0, \quad \nabla \cdot \boldsymbol{u}_{(0)} = 0, \\ (\boldsymbol{u}_{(0)})_t + \nabla \cdot (\boldsymbol{u}_{(0)} \otimes \boldsymbol{u}_{(0)}) + \frac{\nabla p_{(2)}}{\rho_{(0)}} = 0, \end{aligned} \tag{6}$$

or, in conservation form,

$$\mathrm{Diag}\,(1, \ldots, 1, 0)\, \boldsymbol{\omega}_t + \nabla \cdot \boldsymbol{f}^I(\boldsymbol{\omega}) = 0 \qquad \text{with} \qquad \boldsymbol{\omega} := \begin{pmatrix} \boldsymbol{u}_{(0)} \\ p_{(2)} \end{pmatrix} \qquad \text{and} \qquad \boldsymbol{f}^I(\boldsymbol{\omega}) := \begin{pmatrix} \boldsymbol{u}_{(0)} \otimes \boldsymbol{u}_{(0)} + \frac{p_{(2)}}{\rho_{(0)}} \cdot \mathrm{Id} \\ \boldsymbol{u}_{(0)} \end{pmatrix}. \tag{7}$$

The existence of a limit necessitates the use of specially designed initial data, see e.g. [5, 6, 7], which we introduce in the sequel for the isentropic Euler equations:

Definition 1 (Well prepared initial conditions)**.** *We call initial data $\boldsymbol{w}^0$ for the compressible equation* well prepared *if they can be represented by an asymptotic expansion as in (5) and fulfill*

$$\rho^0 = \text{const} + \mathcal{O}(\varepsilon^2), \quad \nabla \cdot \boldsymbol{u}^0 = \mathcal{O}(\varepsilon).$$

Well prepared initial data, together with sufficient smoothness, guarantee the convergence of the solution as $\varepsilon \to 0$ [5].

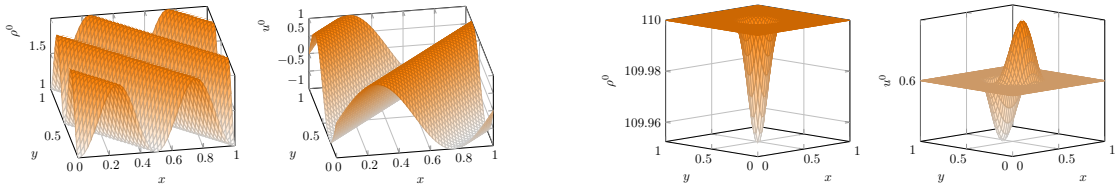

Figure 1: Initial density and $x-$velocity for $\varepsilon = 1$. Left two images: ρ^0 and u^0 of Expl. 1. Right two images: ρ^0 and u^0 of Expl. 2.

Remark 1. *The solution $\boldsymbol{w}_{(0)}$ plays an important role in the development of our splitting, see Sec. 4. To simplify the notation of the proofs, we will from now on denote it as $\boldsymbol{w}_{\text{ref}}$, i.e.,*

$$\boldsymbol{w}_{\text{ref}} := \boldsymbol{w}_{(0)}.$$

Other reference solutions $\boldsymbol{w}_{\text{ref}}$ might be possible, the investigation of this is subject to future research; we do not consider this in further detail here.

2.2. Examples

In the following, we discuss several examples that we are going to use in the numerical results section. For all the examples, we use the domain $\Omega = [0,1] \times [0,1]$, and we assume periodic boundary conditions to neglect the possible influence of effects due to boundary conditions. The focus is on examples that are sufficiently smooth for all ε. A quite well-known test case can be found in [11, 13] for the isentropic Euler equations, but no exact solution is known. Another example is given in Bispen et al. in [9] and is also used in [2]. Contrary to the first example, this one has a known solution which is unfortunately not smooth enough (only C^1). Therefore, we derive a third example, motivated by the second one, which is in C^∞.

Example 1 (Periodic flow [11, 13])**.** *The* periodic flow *is given by a pressure function $p(\rho) = \rho^2$ and periodic initial conditions, shown in Fig. 1 on the left,*

$$\rho(x,y,0) = 1 + \varepsilon^2 \sin(2\pi(x+y)) \sin(2\pi(x+y)), \quad \boldsymbol{u}(x,y,0) = \begin{pmatrix} \sin(2\pi(x-y)) \\ \sin(2\pi(x-y)) \end{pmatrix}.$$

This example has been defined in [11, 13]. Unfortunately, we do not know an analytical solution for this example. An exact solution is known to the second example:

Example 2 (Traveling vortex)**.** *The* traveling vortex *is given by a pressure function $p(\rho) = \frac{1}{2}\rho^2$ and periodic initial conditions, shown in Fig. 1 on the right,*

$$\rho(x,y,0) = 110 + \varepsilon^2 \left(\frac{1.5}{4\pi}\right)^2 \delta(r_c)(k(r_c) - k(\pi)),$$
$$\boldsymbol{u}(x,y,0) = \begin{pmatrix} 0.6 \\ 0 \end{pmatrix} + 1.5(1 + \cos(r_c))\delta(r_c) \begin{pmatrix} (0.5 - y) \\ (x - 0.5) \end{pmatrix}.$$

where

$$k(r) := 2\cos(r) + 2r\sin(r) + \frac{1}{8}\cos(2r) + \frac{1}{4}r\sin(2r) + \frac{3}{4}r^2,$$
$$r_c(x,y) := 4\pi\sqrt{(x-0.5)^2 + (y-0.5)^2}, \quad \delta(r) := \begin{cases} 1 & r < \pi \\ 0 & \text{otherwise} \end{cases}.$$

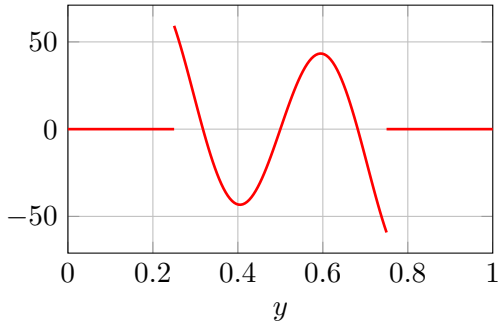

Figure 2: Second derivative of the first velocity component of the initial conditions of the traveling vortex example for a fixed x and variable y, i.e. $\frac{\partial^2}{\partial y^2} u_0 \left(\frac{1}{2}, y\right)$.

This example was introduced by Bispen et al. in [9], based on [47]. Note that earlier work used periodic boundary conditions in one and absorbing boundary conditions in the other direction. An analytic solution is available and given by

$$\rho(x, y, t) = \rho(x - 0.6t, y, 0), \quad \boldsymbol{u}(x, y, t) = \boldsymbol{u}(x - 0.6t, y, 0),$$

thus the vortex is transported in $x-$direction with a velocity of 0.6.

Considering the second derivative in y-direction of the velocity u_0 for a fixed value x, one can see a jump in the derivative, see Fig. 2. This means that the function is not more than one time continuously differentiable, making it not the perfect candidate in a high-order setting. We therefore consider the third example:

Example 3 (High-order vortex)**.** *The* high-order vortex *is given by a pressure function* $p(\rho) = \frac{1}{2}\rho^2$ *and periodic initial conditions*

$$\rho(x, y, 0) = 2 + 250,000\varepsilon^2 \begin{cases} \frac{1}{2} e^{\frac{2}{\Delta r}} \Delta r - \mathrm{Ei}\left(\frac{2}{\Delta r}\right) & r < \frac{1}{2} \\ 0 & \textit{otherwise} \end{cases}$$

$$\boldsymbol{u}(x, y, 0) = \begin{pmatrix} 1/2 \\ 0 \end{pmatrix} + 500 \begin{pmatrix} \frac{1}{2} - y \\ x - \frac{1}{2} \end{pmatrix} \cdot \begin{cases} e^{\frac{1}{\Delta r}} & r < \frac{1}{2} \\ 0 & \textit{otherwise} \end{cases},$$

where $r := \sqrt{(x - \frac{1}{2})^2 + (y - \frac{1}{2})^2}$ *and* $\Delta r := r^2 - \frac{1}{4}$.

This example has been derived for this work by considering a radial symmetric ansatz function for density and an ansatz function that represents a rotation for velocity. The solution is a transport of the vortex in x-direction, i.e.

$$\rho(x, y, t) = \rho\left(x - \frac{1}{2}t, y, 0\right), \quad \boldsymbol{u}(x, y, t) = \boldsymbol{u}\left(x - \frac{1}{2}t, y, 0\right).$$

The high-order vortex can be seen as a high-order extension of Bispen et al.'s work. Note that the vortex is defined with the help of the exponential integral function

$$\mathrm{Ei}(x) := \int_{-\infty}^{x} \frac{e^t}{t} \mathrm{d}t.$$

This exponential integral function is, among others, implemented in the boost package [48, 49], which is used in the implementation.

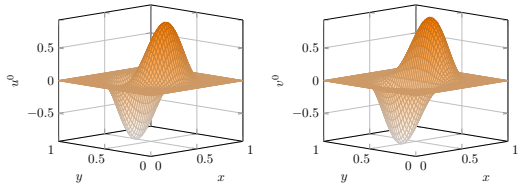

Figure 3: Initial velocity field of the high-order traveling vortex example. Left the initial velocity u^0 in x-direction and right the initial velocity v^0 in y-direction.

3. Desired asymptotic behavior

The goal of the current work is to devise a high-order numerical method for weakly compressible flows. Obviously, the behavior of the method as $\varepsilon \to 0$ is therefore of special interest. In this section, we review appropriate definitions of *asymptotic consistency*, a term coined by Jin, see, e.g., [11, 13, 16, 44] and others. As we are dealing with a high-order method, we have reformulated some of those properties to fit to the underlying setting in the following definition.

Definition 2 (Asymptotic properties)**.**

- *A numerical method is called* asymptotically consistent *(*AC*), see e.g. [44], if its lowest order expansion is a consistent discretization of the limit equation.*
- *A numerical method is called* asymptotic preserving *(*AP*), see e.g. [42, 43, 44], if it is asymptotically consistent and if the limit ("$\varepsilon = 0$") method is a stable discretization of the limit equation* (6).
- *A numerical method is called* asymptotically stable *(*AS*), see e.g. [9], if the numerical solution obtained under a convective CFL condition* (3) *can be bounded by the initial conditions independently of ε.*
- *A numerical method is called* asymptotically accurate *(*AA*), see e.g. [45, 46], if the numerical solution converges towards the exact solution with the correct convergence order for a range of discretization parameters that is independently of ε. The latter means that the phenomenon of order reduction [50, 51] does not occur.*
- *A numerical method is called* asymptotically optimal *(*AO*) if it is* asymptotically consistent*,* asymptotically stable *and* asymptotically accurate*.*

4. The RS-IMEX splitting

As already pointed out in the introduction, the choice of a splitting of the convective flux function $\boldsymbol{f}^C$ is a core ingredient to obtain a stable and efficient numerical method. This work relies on the recently introduced RS-IMEX splitting, see [1, 2, 20]. To introduce the splitting and the basic ideas, we start by considering the simplest of all IMEX frameworks, the IMEX-Euler semi discretization. Applied to (4) with a splitting of the convective flux into

$$\boldsymbol{f}^C(\boldsymbol{w}) = \widehat{\boldsymbol{f}^C}(\boldsymbol{w}) + \widetilde{\boldsymbol{f}^C}(\boldsymbol{w}), \tag{8}$$

yields

$$\boldsymbol{w}^{n+1} - \boldsymbol{w}^n + \Delta t \nabla \cdot \left(\widetilde{\boldsymbol{f}^C}(\boldsymbol{w}^{n+1}) + \widehat{\boldsymbol{f}^C}(\boldsymbol{w}^n) \right) = 0. \tag{9}$$

Note that $\widetilde{\boldsymbol{f}^C}$ is the part that is treated implicitly, while $\widehat{\boldsymbol{f}^C}$ is the part that is treated explicitly. In the following the upper index n of $\boldsymbol{w}^n$ corresponds to the numerical solution - with respect to time - at time instance

$$t^n := n \cdot \Delta t.$$

(Uniform time slabs are not a necessity.) To obtain the splitting, the RS-IMEX idea is to linearize the flux function $\boldsymbol{f}^C$ around a precomputed or exactly given *reference solution* $\boldsymbol{w}_{\text{ref}}$ for the implicit part. This reference solution is given in Rem. 1 for the isentropic Euler equations. For a more detailed derivation of the RS-IMEX splitting we refer to [1, 2]. Let us note that similar splitting ideas have also been used in [22] for the stiff collision operator of kinetic equations and in [9, 21] for a perturbation around the lake at rest of the shallow water equations. More formally the RS-IMEX splitting is given in the following definition.

Definition 3 (RS-IMEX)**.** *The* RS-IMEX *splitting is defined by*

$$\begin{aligned}
\widetilde{\boldsymbol{f}^C}(\boldsymbol{w}) &= \boldsymbol{f}^C(\boldsymbol{w}_{\text{ref}}) + \partial_{\boldsymbol{w}} \boldsymbol{f}^C(\boldsymbol{w}_{\text{ref}}) \cdot (\boldsymbol{w} - \boldsymbol{w}_{\text{ref}}),\\
\widehat{\boldsymbol{f}^C}(\boldsymbol{w}) &= \boldsymbol{f}^C(\boldsymbol{w}) - \widetilde{\boldsymbol{f}^C}(\boldsymbol{w}) = \boldsymbol{f}^C(\boldsymbol{w}) - \boldsymbol{f}^C(\boldsymbol{w}_{\text{ref}}) - \partial_{\boldsymbol{w}} \boldsymbol{f}^C(\boldsymbol{w}_{\text{ref}}) \cdot (\boldsymbol{w} - \boldsymbol{w}_{\text{ref}}),
\end{aligned}$$

where $\boldsymbol{w}_{\text{ref}}$ denotes the reference solution, given in Rem. 1. $\partial_{\boldsymbol{w}} \boldsymbol{f}^C$ denotes the Jacobian of $\boldsymbol{f}^C$, $\widetilde{\boldsymbol{f}^C}$ is handled implicitly and $\widehat{\boldsymbol{f}^C}$ is handled explicitly.

By the definition of the splitting one can directly obtain that the implicit part is linear and therefore the resulting system can be solved efficiently by a linear solution technique. Note that, although the idea stems from a linearization, there is no first-order linearization error of the flux, because remaining terms are collected in $\widehat{\boldsymbol{f}^C}$. Applying the definition of $\boldsymbol{f}^C$ given in (4), one can directly compute the flux functions $\widehat{\boldsymbol{f}^C}$ and $\widetilde{\boldsymbol{f}^C}$ for the isentropic Euler equations.

Definition 4 (RS-IMEX splitting for the isentropic Euler equations)**.** *The RS-IMEX splitting for the isentropic Euler equations is given by*

$$\begin{aligned}
\widehat{\boldsymbol{f}^C}(\rho, \rho\boldsymbol{u}) &= \begin{pmatrix} 0 \\ \rho(\boldsymbol{u} - \boldsymbol{u}_{\text{ref}}) \otimes (\boldsymbol{u} - \boldsymbol{u}_{\text{ref}}) + \frac{1}{\varepsilon^2} \left(p(\rho) - p(\rho_{\text{ref}}) - p'(\rho_{\text{ref}})(\rho - \rho_{\text{ref}})\right) \cdot \text{Id} \end{pmatrix}\\
\widetilde{\boldsymbol{f}^C}(\rho, \rho\boldsymbol{u}) &= \begin{pmatrix} \rho\boldsymbol{u} \\ -\rho\boldsymbol{u}_{\text{ref}} \otimes \boldsymbol{u}_{\text{ref}} + \rho\boldsymbol{u} \otimes \boldsymbol{u}_{\text{ref}} + \rho\boldsymbol{u}_{\text{ref}} \otimes \boldsymbol{u} + \frac{1}{\varepsilon^2} \left(p(\rho_{\text{ref}}) + p'(\rho_{\text{ref}})(\rho - \rho_{\text{ref}})\right) \cdot \text{Id} \end{pmatrix}.
\end{aligned}$$

Remark 2. *Note that the RS-IMEX splitting idea as given in Def. 3 can directly be extended to a wide range of different equations. However, the best way to compute the reference solution, if it is not given analytically, is not directly clear and depends on the given equation and the used numerical method, see Sec. 6 for more details in the given setting. Furthermore, it is not imminent that this splitting always yields a stable method.*

Remark 3. *1. The eigenvalues in the two-dimensional case of $\partial_{\boldsymbol{w}} \widehat{\boldsymbol{f}^C}(\boldsymbol{w}) \cdot \boldsymbol{n}$ of are given by*

$$\boldsymbol{\lambda} = \begin{pmatrix} 0 \\ 2(\boldsymbol{u} - \boldsymbol{u}_{\text{ref}})^T \\ (\boldsymbol{u} - \boldsymbol{u}_{\text{ref}})^T \end{pmatrix} \cdot \boldsymbol{n}$$

2. The in magnitude largest eigenvalues of the Jacobian of the implicit part are in $\mathcal{O}\left(\frac{1}{\varepsilon}\right)$.

We can conclude two different things from Rem. 3. First, the stiffness of the equation is completely hidden in the implicit part. Second, if we take the limit $\varepsilon \to 0$ and assume that the solution and the reference solution will eventually coincide, the explicit part vanishes.

5. The IMEX DG method

In the previous section we briefly presented the RS-IMEX splitting idea in the context of an IMEX-Euler discretization, see (9). The extension to higher-order methods is evident, methods of choise are, e.g., high-order IMEX Runge-Kutta methods [27, 28, 29, 30, 31, 32, 33] or high-order IMEX linear multistep methods [24, 25, 26]. High-order temporal integration has to be coupled to a high-order spatial discretization, e.g. one could use spectral volume [52, 53], spectral difference [54] or discontinuous Galerkin methods [34, 35, 36, 37, 38]. The method of choice for this work is a combination of a high-order IMEX Runge-Kutta method with a high-order discontinuous Galerkin discretization, yielding an IMEX DG method [39, 40, 41].

5.1. Preliminary definitions

We assume that Ω is divided into non-overlapping cells Ω_k as

$$\bigcup_{k=1}^{\mathrm{ne}} \overline{\Omega_k} = \Omega \qquad \text{and} \qquad \Omega_k \cap \Omega_i = \emptyset \quad \forall k \neq i.$$

The boundary of the cell Ω_k is denoted by $\partial\Omega_k$ and n_k denotes the corresponding outward normal vector. For a value of $x \in \partial\Omega_k$, we define the interior (I) and exterior (E) value, respectively, of a function σ by

$$\sigma_I(x) := \lim_{0<\delta\to 0} \sigma(x - \delta n_k) \qquad \text{and} \qquad \sigma_E(x) := \lim_{0<\delta\to 0} \sigma(x + \delta n_k). \tag{10}$$

If a boundary is considered independently of a specific cell, we can in a similar way define a value of σ_I and σ_E based on an arbitrary, but fixed direction of edge normal vectors. On domain Ω with triangulation $\{\Omega_k\}$ we define a broken polynomial space by

$$V_q := \{v \in L^2(\Omega) \ : \ v_{|\Omega_k} \in \mathbb{P}_q(\Omega_k) \ \forall \ k = 1, \ldots, \mathrm{ne}\},$$

where $\mathbb{P}_q(\Omega_k)$ are all polynomial functions with maximum degree q on cell Ω_k. Of course an adaptive choice of q is possible. To also take time into account, we assume that the temporal domain is given by $[0, T]$ with $T \in \mathbb{R}^+$. This time domain is split into N time instance $t^n = n\Delta t$,

$$0 = t^0 < \ldots < t^n < \ldots < t^N = T.$$

5.2. Discontinuous Galerkin method for compressible flows

Following the common steps [38], a DG discretization of (1) is given in the following definition:

Definition 5 (DG)**.** *We seek the function $\boldsymbol{w}_{\Delta x} \in V_q^d$ which fulfills*

$$\int_{\Omega_k} (\boldsymbol{w}_{\Delta x})_t \cdot \varphi \mathrm{d}x - \int_{\Omega_k} \boldsymbol{f}^C(\boldsymbol{w}_{\Delta x}) \cdot \nabla\varphi \mathrm{d}x + \int_{\partial\Omega_k} \boldsymbol{h}(\boldsymbol{w}_{I,\Delta x}, \boldsymbol{w}_{E,\Delta x})\varphi \cdot \boldsymbol{n} \mathrm{d}s = 0,$$

where $\boldsymbol{h}$ denotes the numerical flux function, for all functions $\varphi \in V_q$ on every cell Ω_k. (Reminder: It is $\boldsymbol{f}^C(\boldsymbol{w}) \in \mathbb{R}^{d\times 2}$, q is polynomial degree of ansatz functions.)

This variational formulation is continuous with respect to the time variable and discrete with respect to the spatial variable. In the following, a lower index Δx denotes a spatial discretization. There are many possible choices for a numerical flux function, but, as we observed in [2] and also as described by Bispen et al. in [9], the choice of the numerical flux function affects the asymptotic consistency. At this instance

we keep the choice of the numerical flux function rather general and consider the following class of fluxes in viscosity form:

$$\boldsymbol{h}(\boldsymbol{w}_I, \boldsymbol{w}_E) := \frac{1}{2}\left(\boldsymbol{f}^C(\boldsymbol{w}_I) + \boldsymbol{f}^C(\boldsymbol{w}_E)\right) + \frac{1}{2}\,\mathrm{Diag}\,(\alpha_1, \ldots, \alpha_d)\,(\boldsymbol{w}_I - \boldsymbol{w}_E)\cdot\boldsymbol{n}, \tag{11}$$

where every equation can be stabilized with its own stabilization coefficient α_i, $i = 1, \ldots, d$. Note that choosing the maximal absolute eigenvalue as the stabilization coefficient for every equation, i.e. $\alpha_i = \alpha_j$ for $i, j = 1 \ldots d$, results in the Rusanov numerical flux function (also called local Lax-Friedrichs numerical flux function) [55]. The choice of the stabilization coefficients is done in Sec. 6.

5.3. Discontinuous Galerkin method for incompressible flows

The RS-IMEX approach is based on the reference solution, which is in fact the solution of the limit equation (7). Compared with its compressible counterpart, one equation is replaced by the algebraic (w.r.t. to time) equation

$$\nabla \cdot \boldsymbol{u} = 0.$$

In order to discretize this equation we use a similar variational formulation as before and stabilize this equation in the quasi-pressure $p_{(2)}$. This results in the following method.

Definition 6. *We seek the function $\boldsymbol{\omega}_{\Delta x} \in V_q^d$ which fulfills*

$$\mathrm{Diag}\,(1, \ldots, 1, 0)\cdot\int_{\Omega_k}(\boldsymbol{\omega}_{\Delta x})_t\cdot\varphi \mathrm{d}x - \int_{\Omega_k}\boldsymbol{f}^I(\boldsymbol{\omega}_{\Delta x})\cdot\nabla\varphi \mathrm{d}x + \int_{\partial\Omega_k}\boldsymbol{h}(\boldsymbol{\omega}_{I,\Delta x}, \boldsymbol{\omega}_{E,\Delta x})\varphi\cdot\boldsymbol{n}\mathrm{d}s = 0,$$

for all functions $\varphi \in V_q$ on every cell Ω_k. $\boldsymbol{h}$ is again a numerical flux function as in (11) with $\boldsymbol{f}^C$ replaced by $\boldsymbol{f}^I$ and with a different choice for the stabilization coefficients. (Details in Sec. 6.)

Note that since the pressure $p_{(2)}$ only occurs with its spatial derivative, it is not unique. Therefore we assume that the pressure is mean value free, i.e.,

$$\int_\Omega p_{(2)}\mathrm{d}x = 0.$$

To enforce this we perform a pressure correction after every time step in order to neglect possible mean values.

Remark 4. *In principle, we could also use a method off-the-shelf for the incompressible equation, see, e.g., [56]. The reason why we favour the method given above will be clarified in Thm. 2. Roughly speaking, the method presented in Def. 6, equipped with suitable time integration, is the $\varepsilon = 0$ limit of the method in Def. 5, again equipped with time integration.*

5.4. IMEX Runge-Kutta methods

In Sec. 4 we have presented the RS-IMEX approach which splits the flux function $\boldsymbol{f}^C$ into an explicit part, denoted by $\widehat{\boldsymbol{f}^C}$, and an implicit part, denoted with $\widetilde{\boldsymbol{f}^C}$. Here, we extend the IMEX-Euler to IMEX Runge-Kutta methods, see e.g. [27].

In this work we do not consider an arbitrary IMEX Runge-Kutta method, we restrict ourselves to a (relatively large) subclass which we identified as important in our previous work [1]. The following remark clarifies the methods we use.

Remark 5. *1. We only consider IMEX Runge-Kutta methods which are* globally stiffly accurate *(GSA), see e.g. [28]. In short this is fulfilled if the update step is equal to the last internal stage of the Runge-Kutta method. This corresponds to the* first same as last *property for an explicit and the* stiffly accurate *property for an implicit Runge-Kutta method. As our system is autonomous, the IMEX Runge-Kutta methods are fully defined by the two Butcher tableaux $\widetilde{A}$ and $\widehat{A}$.*

2. We only consider IMEX Runge-Kutta methods where the implicit matrix $\widetilde{A}$ is a lower triangular one, such that in every internal stage only one implicit variable occurs.

3. We only consider IMEX Runge-Kutta methods of type A or type CK. This is given if the implicit matrix $\widetilde{A}$ is invertible (type A) or the first entry of the implicit matrix equals to 0 and the remaining submatrix is invertible (type CK). See Def. 7 for more details. For a more detailed classification of IMEX Runge-Kutta methods we refer to [51].

Consequently, we can define the following $s-$stage IMEX Runge-Kutta methods used in this work:

Definition 7 (GSA IMEX Runge-Kutta scheme)**.** *For every $t^{n+1} = t^n + \Delta t$ do the following:*

1. For $i = 1, \dots, s$ solve

$$\boldsymbol{w}^{n,i} - \boldsymbol{w}^n + \Delta t \left(\sum_{j=1}^{i} \widetilde{A}_{i,j} \nabla \cdot \widetilde{\boldsymbol{f}^C}(\boldsymbol{w}^{n,j}) + \sum_{j=1}^{i-1} \widehat{A}_{i,j} \nabla \cdot \widehat{\boldsymbol{f}^C}(\boldsymbol{w}^{n,j}) \right) = 0, \tag{12}$$

where $\boldsymbol{w}^{n,i}$ denotes solution of the i^{th} internal stage.

2. Set $\boldsymbol{w}^{n+1} = \boldsymbol{w}^{n,s}$.

The coefficients of the IMEX RK method are given by two Butcher tableaux, the one with overhats referring to the explicit, the other to the implicit part. Because of our restrictions on the Runge-Kutta method (see Rem. 5), the implicit coefficient matrix has to fulfill $\widetilde{A}_{ii} \neq 0$ for $i = 2 \dots s$. For a type A method, there even holds $\widetilde{A}_{11} \neq 0$ in addition.

Based on our work in [1], we use the IMEX Runge-Kutta methods presented in Tbl. 2, 3, 4 and 5, originally presented in [27, 28, 32, 33]. A classification of these methods can be seen in Tbl. 1.

	IMEX-Euler	*IMEX-DPA-242*	*IMEX-BPR-353*	*IMEX-ARK-4A2*
Order	1	2	3	4
GSA	Yes	Yes	Yes	Yes
Type	CK	A	CK	CK

Table 1: Classification of the used IMEX Runge-Kutta methods concerning their order, structure and type.

6. Asymptotic behavior of the numerical method

So far, we have left out the details on the numerical flux function. We will fix those details in this section in such a way that the method to be presented is asymptotically consistent. Let us begin by giving a short overview on the notation.

Remark 6 (Notation)**.** *1. An upper index n, e.g., $\boldsymbol{u}^n$, indicates that the quantity is given at time level $t = t^n$.*

2. *An additional upper index i, e.g., $\boldsymbol{u}^{n,i}$, denotes the i^{th} internal stage of an IMEX Runge-Kutta method.*

3. *A lower index Δx, e.g., $\boldsymbol{u}_{\Delta x}$ denotes a variable which belongs to a discontinuous Galerkin discretization.*

4. *An additional lower index I or E, e.g., $\boldsymbol{u}_{I,\Delta x}$ denotes the interior or exterior value corresponding to an edge, see (10).*

5. *A lower index in brackets (i), e.g., $\boldsymbol{u}_{(i)}$, denotes a variable which belongs to the i^{th} component of an asymptotic expansion, see (5)*

6. *A lower index* ref*, e.g., $\boldsymbol{u}_{\text{ref}}$, denotes the reference solution, see Rem. 1*

6.1. Asymptotic consistency

As mentioned in Sec. 3, our aim is to develop a method whose $\varepsilon \to 0$ limit is a consistent discretization of the limit equation (6). In the following, we prove this property, thereby identifying suitable viscosity parameters in (11). For the ease of presentation, we work in two steps: As mentioned before the numerical method is desired to preserve the asymptotic behavior of the corresponding equation. Therefore the limit numerical method is desired to be a consistent discretization of the limit equation. In the following we prove this property for two cases:

1. First, we consider the semi discrete (discrete in time) setting.
2. Then, we consider the fully discrete setting, where the DG method is coupled to an IMEX Runge-Kutta method.

6.1.1. Semi discrete setting

We start by considering the RS-IMEX splitting for the isentropic Euler equation (1) coupled to an IMEX Runge-Kutta temporal discretization as in (12).

Lemma 1. *The internal stage $\boldsymbol{w}^{n,i}$ of the RS-IMEX method coupled to an IMEX Runge-Kutta temporal discretization (see (12)) is asymptotically consistent, if all previous internal stages and the previous time instance $\boldsymbol{w}^n$ are well prepared in the sense of Def. 1 and there holds $\rho^n_{(0)} = \rho_{\text{ref}}$.*

Proof. We assume that all the quantities can be represented with an asymptotic expansion as in (5). If $\widetilde{A}_{1,1} = 0$, which happens for type CK methods, then the first internal stage is equal to the previous time instance $\boldsymbol{w}^n_{\Delta x}$. It is therefore directly well prepared. Therefore, we consider the i^{th} internal stage with $\widetilde{A}_{ii} \neq 0$.

Because the numerical density is constant up to $\mathcal{O}(\varepsilon^2)$, we know that its zeroth-order expansion is equal to the reference density ρ_{ref}. Therefore, considering the $\mathcal{O}(\varepsilon^{-2})$ terms of the momentum equation, we obtain

$$\begin{aligned} 0 =& \nabla \frac{\widetilde{A}_{i,i}}{\varepsilon^2} \left(p(\rho_{\text{ref}}) + p'(\rho_{\text{ref}})(\rho^{n,i}_{(0)} - \rho_{\text{ref}}) \right) \\ \Leftrightarrow\ 0 =& \nabla \frac{\widetilde{A}_{i,i}}{\varepsilon^2} \left(p'(\rho_{\text{ref}})\rho^{n,i}_{(0)}) \right) \\ \Leftrightarrow\ 0 =& \nabla \rho^{n,i}_{(0)}. \end{aligned}$$

Thus the limit density is constant in space. Next we consider the $\mathcal{O}(1)$ terms of the first equation and integrate over the whole domain. Using the periodic boundary conditions we get

$$\int_\Omega \rho^{n,i}_{(0)} - \rho^n_{(0)} \mathrm{d}x = 0.$$

Since both values are constant in space, we can conclude that $\rho_{(0)}^{n,i}$ is constant in i, and therefore it is equal to ρ_{ref}. Considering again the $\mathcal{O}(1)$ terms of the mass equation we now obtain

$$\sum_j \widetilde{A}_{ij} \nabla \cdot (\rho \boldsymbol{u})_{(0)}^{n,j} = 0.$$

Since the previous stages are well prepared, which means that their momentum is solenoidal, we directly obtain $\nabla \cdot (\rho \boldsymbol{u})_{(0)}^{n,i} = 0$ if $\widetilde{A}_{ii} \neq 0$. The proof is finalized by the remark that the discrete limit momentum equation is a consistent discretization of the limit momentum equation. □

Theorem 1. *The RS-IMEX method coupled to an IMEX Runge-Kutta temporal discretization as given in Rem. 5 and Def. 7 is asymptotically consistent if well prepared initial data are used.*

Proof. The theorem follows directly from Lem. 1, the well prepared initial data and the GSA property of the used IMEX Runge-Kutta method. □

A question which arises from the usage of the RS-IMEX splitting is how to compute the limit solution. In an ideal case this solution is given, but generally we need a numerical method for its computation. It is useful to compute the limit solution in such a way that it corresponds to the solution of the limit method.

Theorem 2. *The limit of the semi discrete method (12) is a discretization that is fully implicit-in-time.*

Proof. Upon adding a zero as

$$\rho_{\text{ref}} \boldsymbol{u}_{(0)}^{n,j} \otimes \boldsymbol{u}_{(0)}^{n,j} - \rho_{\text{ref}} \boldsymbol{u}_{(0)}^{n,j} \otimes \boldsymbol{u}_{(0)}^{n,j},$$

the limit numerical method reads (see also Def. 4)

$$\begin{pmatrix} 0 \\ \rho_{\text{ref}} \boldsymbol{u}_{(0)}^{n,i} \end{pmatrix} = \begin{pmatrix} 0 \\ \rho_{\text{ref}} \boldsymbol{u}_{(0)}^{n} \end{pmatrix}$$
$$-\Delta t \sum_j \widehat{A}_{ij} \nabla \cdot \begin{pmatrix} 0 \\ \rho_{\text{ref}} (\boldsymbol{u}_{(0)}^{n,j} - \boldsymbol{u}_{\text{ref}}^{n,j}) \otimes (\boldsymbol{u}_{(0)}^{n,j} - \boldsymbol{u}_{\text{ref}}^{n,j}) + \left(p_{(2)}^{n,j} - p'(\rho_{\text{ref}}) \rho_{(2)}^{n,j} \right) \cdot \text{Id} \end{pmatrix}$$
$$-\Delta t \sum_j \widetilde{A}_{ij} \nabla \cdot \begin{pmatrix} \boldsymbol{u}_{(0)}^{n,j} \\ -\rho_{\text{ref}} (\boldsymbol{u}_{(0)}^{n,j} - \boldsymbol{u}_{\text{ref}}^{n,j}) \otimes (\boldsymbol{u}_{(0)}^{n,j} - \boldsymbol{u}_{\text{ref}}^{n,j}) + \rho_{\text{ref}} \boldsymbol{u}_{(0)}^{n,j} \otimes \boldsymbol{u}_{(0)}^{n,j} + p'(\rho_{\text{ref}}) \rho_{(2)}^{n,j} \cdot \text{Id} \end{pmatrix}.$$

Now, for the moment, we assume that for all previous internal stages, the numerical solution and the reference solution coincide. Furthermore, from the asymptotic expansion one concludes

$$p_{(2)}^{n,i} = p'(\rho_{\text{ref}}) \rho_{(2)}^{n,i}.$$

Finally, this simplifies to

$$\begin{pmatrix} 0 \\ \rho_{\text{ref}} \boldsymbol{u}_{(0)}^{n,i} \end{pmatrix} = \begin{pmatrix} 0 \\ \rho_{\text{ref}} \boldsymbol{u}_{(0)}^{n} \end{pmatrix} + \Delta t \widetilde{A}_{ii} \nabla \cdot \begin{pmatrix} \boldsymbol{u}_{(0)}^{n,i} \\ -\rho_{\text{ref}} (\boldsymbol{u}_{(0)}^{n,i} - \boldsymbol{u}_{\text{ref}}^{n,i}) \otimes (\boldsymbol{u}_{(0)}^{n,i} - \boldsymbol{u}_{\text{ref}}^{n,i}) + \rho_{\text{ref}} \boldsymbol{u}_{(0)}^{n,i} \otimes \boldsymbol{u}_{(0)}^{n,i} + p_{(2)}^{n,i} \cdot \text{Id} \end{pmatrix},$$

which is a fully implicit discretization of the incompressible equation with additional terms in $(\boldsymbol{u}_{(0)}^{n,i} - \boldsymbol{u}_{\text{ref}}^{n,i})$. If therefore $\boldsymbol{u}_{\text{ref}}^{n,i}$ has been computed by the fully implicit method (which amounts to taking only the implicit part of the IMEX Runge-Kutta method), the two solutions correspond to each other. □

Remark 7. *Theorem 2 is the reason why we discretise the reference solution using a fully implicit scheme. Similar reasoning also holds true for the fully discrete case, where space is discretised using the discontinuous Galerkin discretization.*

6.1.2. Fully discrete setting

Here, we consider the fully discrete setting, i.e., temporal discretization with an IMEX Runge-Kutta method and spatial discretization with a DG method. To clarify the choice of the numerical diffusion coefficients in (11), we start with the following lemma:

Lemma 2. *Let the function $\sigma_{\Delta x} \in V_q$ be such that*

$$\int_{\partial\Omega_k} (\sigma_{I,\Delta x} - \sigma_{E,\Delta x})\varphi \mathrm{d}s = 0, \qquad \forall \varphi \in V_q, \forall k = 1, \dots, \mathrm{ne}\,. \tag{13}$$

Then, $\sigma_{\Delta x}$ is continuous.

Proof. We can choose $\varphi = \sigma_{\Delta x}$ in (13) and obtain

$$\int_{\partial\Omega_k} (\sigma_{I,\Delta x} - \sigma_{E,\Delta x})\sigma_{I,\Delta x} \mathrm{d}s = 0$$

on every cell Ω_k. Summing up over the whole domain and rearranging terms leads to

$$0 = \sum_k \int_{\partial\Omega_k} (\sigma_{I,\Delta x} - \sigma_{E,\Delta x})\sigma_{I,\Delta x} \mathrm{d}s = \sum_e \int_e (\sigma_{I,\Delta x} - \sigma_{E,\Delta x})^2 \mathrm{d}s.$$

This means that $\sigma_{I,\Delta x} = \sigma_{E,\Delta x}$ and therefore the quantity $\sigma_{\Delta x}$ is continuous over every cell boundary. □

This lemma has a direct consequence for the numerical solution. Namely, if we can show that the numerical stabilization of one quantity lives on a different scale (with respect to ε) than the rest of the corresponding equation, the $\varepsilon = 0$ limit of this quantity is continuous. Since the choice of the implicit stabilization coefficient $\widetilde{\alpha}$ is still open, we are able to influence the continuity of the corresponding limit solution. We know from Sec. 2 that the limit density is constant up to $\mathcal{O}(\varepsilon^2)$. Enforcing its continuity therefore makes sense, which is why we define the numerical viscosity as follows:

Definition 8. *We define the numerical stabilization coefficients in (11) as*

$$\widetilde{\alpha} := \mathrm{Diag}\left(\frac{1}{\varepsilon^2}, 1, \dots, 1\right) \qquad \textit{and} \qquad \widehat{\alpha} := 2 \cdot \varepsilon.$$

Remark 8.

- *The choice of $\widehat{\alpha}$ is motivated by Rem. 3, as the eigenvalues of $\partial_{\boldsymbol{w}} \widehat{\boldsymbol{f}^C}(\boldsymbol{w}) \cdot \boldsymbol{n}$ are in $\mathcal{O}(\varepsilon)$ if one assumes that $\boldsymbol{u} = \boldsymbol{u}_{\mathrm{ref}} + \mathcal{O}(\varepsilon)$.*
- *Let us note that a somewhat similar choice of the artificial viscosity, for the equations in primitive variables, has been made in [57], motivated by the fundamental work of Turkel [58], who introduced preconditioning of the time derivative to enhance steady-state computations for low-Mach flows.*

With this choice we follow the same steps as for the semi discrete case and start by proving that if all previous internal stages are well prepared, then the algorithm is also asymptotically consistent.

Lemma 3. *The internal stage $\boldsymbol{w}_{\Delta x}^{n,i}$ of the RS-IMEX DG method with an arbitrary polynomial degree $q \geq 0$ and an IMEX Runge-Kutta time integration as given in Rem. 5 and Def. 7 fulfills $\rho_{(0),\Delta x}^{n,i} = \rho_{\mathrm{ref}} + \mathcal{O}(\varepsilon^2)$, and $\nabla \cdot u = 0$ in a discrete sense, see (14) (i.e., it is well prepared in a discrete sense) if all the previous internal stages and the previous time instances are also discretely well prepared, and there holds that $\rho_{\Delta x}^n = \rho_{\mathrm{ref}} + \mathcal{O}(\varepsilon^2)$.*

Proof. Note that if $\widetilde{A}_{1,1} = 0$ then the first internal stage is equal to the previous time instance $\boldsymbol{w}^n_{\Delta x}$, thus it is directly well prepared. Therefore we now consider a given i such that $\widetilde{A}_{i,i} \neq 0$. We assume that every quantity can be expressed by an asymptotic expansion as in (5), e.g.,

$$\begin{pmatrix} \rho^n_{\Delta x} \\ (\rho \boldsymbol{u})^n_{\Delta x} \end{pmatrix} = \begin{pmatrix} \rho^n_{\Delta x,(0)} \\ (\rho \boldsymbol{u})^n_{\Delta x,(0)} \end{pmatrix} + \varepsilon \begin{pmatrix} \rho^n_{\Delta x,(1)} \\ (\rho \boldsymbol{u})^n_{\Delta x,(1)} \end{pmatrix} + \varepsilon^2 \begin{pmatrix} \rho^n_{\Delta x,(2)} \\ (\rho \boldsymbol{u})^n_{\Delta x,(2)} \end{pmatrix} + \mathcal{O}(\varepsilon^3).$$

Due to the numerical stabilization the only terms in $\mathcal{O}(\varepsilon^{-2})$ in the momentum equation are the pressure terms, thus

$$\begin{aligned} 0 =& \widetilde{A}_{i,i} \int_{\Omega_k} \left(p(\rho_{\text{ref}}) + p'(\rho_{\text{ref}})(\rho^{n,i}_{\Delta x,(0)} - \rho_{\text{ref}}) \right) \nabla \varphi \mathrm{d}x \\ & - \widetilde{A}_{i,i} \frac{1}{2} \int_{\partial \Omega_k} \left(p(\rho_{\text{ref}}) + p'(\rho_{\text{ref}})(\rho^{n,i}_{I,\Delta x,(0)} - \rho_{\text{ref}}) + p(\rho_{\text{ref}}) + p'(\rho_{\text{ref}})(\rho^{n,i}_{E,\Delta x,(0)} - \rho_{\text{ref}}) \right) \varphi \boldsymbol{n} \mathrm{d}x \end{aligned}$$

for every test-function φ. Note that we have directly used the fact that the initial values and all previous stages are well prepared. Therefore, there are no explicit contributions. Using integration by parts and changing signs leads to

$$\begin{aligned} 0 =& \widetilde{A}_{i,i} \int_{\Omega_k} \nabla \left(p(\rho_{\text{ref}}) + p'(\rho_{\text{ref}})(\rho^{n,i}_{\Delta x,(0)} - \rho_{\text{ref}}) \right) \varphi \mathrm{d}x \\ & - \widetilde{A}_{i,i} \frac{1}{2} \int_{\partial \Omega_k} \left(p(\rho_{\text{ref}}) + p'(\rho_{\text{ref}})(\rho^{n,i}_{I,\Delta x,(0)} - \rho_{\text{ref}}) - p(\rho_{\text{ref}}) - p'(\rho_{\text{ref}})(\rho^{n,i}_{E,\Delta x,(0)} - \rho_{\text{ref}}) \right) \varphi \boldsymbol{n} \mathrm{d}s \\ =& \widetilde{A}_{i,i} \int_{\Omega_k} \nabla p'(\rho_{\text{ref}}) \rho^{n,i}_{\Delta x,(0)} \varphi \mathrm{d}x - \widetilde{A}_{i,i} \frac{1}{2} \int_{\partial \Omega_k} p'(\rho_{\text{ref}})(\rho^{n,i}_{I,\Delta x,(0)} - \rho^n_{E,\Delta x,(0)}) \varphi \boldsymbol{n} \mathrm{d}s. \end{aligned}$$

Due to La. 2 and the choice of the implicit stabilization, which is in $\mathcal{O}(\varepsilon^{-2})$ for the first equation, we know that $\rho^{n,i}_{\Delta x,(0)}$ is continuous over the cell boundary of Ω_k. Therefore we obtain

$$0 = \int_{\Omega_k} \nabla \rho^{n,i}_{\Delta x,(0)} \varphi \mathrm{d}x.$$

This holds true on every cell Ω_k and for every test-function φ and therefore $\rho^{n,i}_{\Delta x,(0)}$ must be a cell-wise constant. Since it is also continuous it is constant over the whole domain. Similarly, one can also conclude that $\rho^{n,i}_{\Delta x,(1)}$ is constant over the whole domain. Next we consider the $\mathcal{O}(1)$ terms of the conservation of mass equation. Note that, because this part is purely implicit, the reference solution does not occur:

$$\begin{aligned} 0 =& \int_{\Omega_k} \left(\rho^{n,i}_{\Delta x,(0)} - \rho^n_{\Delta x,(0)} \right) \varphi \mathrm{d}x \\ & - \Delta t \sum_j \widetilde{A}_{i,j} \left(\int_{\Omega_k} \rho^{n,j}_{\Delta x,(0)} \boldsymbol{u}^{n,j}_{\Delta x,(0)} \cdot \nabla \varphi \mathrm{d}x - \right. \\ & \left. \frac{1}{2} \int_{\partial \Omega_k} \left(\rho^{n,j}_{\Delta x,(0)} \boldsymbol{u}^{n,j}_{I,\Delta x,(0)} + \rho^{n,j}_{\Delta x,(0)} \boldsymbol{u}^{n,j}_{E,\Delta x,(0)} \right) \boldsymbol{n} \varphi \mathrm{d}s - \frac{1}{2} \int_{\partial \Omega_k} \left(\rho^{n,j}_{I,\Delta x,(2)} - \rho^{n,j}_{E,\Delta x,(2)} \right) \varphi \mathrm{d}s \right). \end{aligned}$$

With the help of periodicity we can now choose $\varphi \equiv 1$ as the test function and summing over the whole domain. This leads to

$$0 = \left(\rho^{n,i}_{\Delta x,(0)} - \rho^n_{\Delta x,(0)} \right) |\Omega|.$$

Consequently, $\rho^{n,i}_{\Delta x,(0)}$ is also constant in time and is equal to ρ_{ref} because of the requirements on the previous stages and initial conditions. Considering again conservation of mass, this equation can now be written as

$$0 = -\sum_j \widetilde{A}_{i,j} \left(\int_{\Omega_k} \rho_{\text{ref}} \boldsymbol{u}^{n,j}_{\Delta x,(0)} \cdot \nabla \varphi \mathrm{d}x - \right. \tag{14}$$

$$\left. \frac{1}{2} \int_{\partial\Omega_k} \left(\rho_{\text{ref}} \boldsymbol{u}^{n,j}_{I,\Delta x,(0)} + \rho_{\text{ref}} \boldsymbol{u}^{n,j}_{E,\Delta x,(0)} \right) \boldsymbol{n} \varphi \mathrm{d}s - \frac{1}{2} \int_{\partial\Omega_k} \left(\rho^{n,j}_{I,\Delta x,(2)} - \rho^{n,j}_{E,\Delta x,(2)} \right) \varphi \mathrm{d}s \right). \tag{15}$$

This is a consistent discretization of $\nabla \cdot \boldsymbol{u} = 0$ with stabilization terms in $\rho^{n,i}_{\Delta x,(2)}$. This is very similar to the discretization of the limit equation where the stabilization is in quasi-pressure, since there holds $p^{n,i}_{\Delta x,(2)} = \gamma \kappa {\rho_{\text{ref}}}^{\gamma-1} \rho^{n,i}_{\Delta x,(2)}$. As for the semi discrete case, it is straightforward to see that the limit momentum equation is a consistent discretization of the corresponding equation. Thus the method is asymptotically consistent with the special choice of the numerical stabilization made in Def. 8. □

This section is finalized with some remarks:

Remark 9.

- *The choice of the numerical flux function is essential for the previous theorem. Taking implicit stabilization coefficients in $\mathcal{O}(1)$, periodic boundary conditions and polynomial degree $q = 0$ results in a method which is not guaranteed to be AC. In [2], this problem has been solved by using a different type of boundary condition, based on the work of [13]. In [59], this problem is solved by adding implicit diffusion to the mass equation, which is similar to the choice of the numerical flux functions presented in this work.*

- *The discretization method of the reference solution has been left open up to this point. From Thm. 2 we know that in the semi discrete setting the limit method corresponds to a fully implicit method. The same holds true - with the same arguments - for the fully discrete setting. The stabilization coefficients for the divergence equation are chosen as $\left(\gamma \kappa {\rho_{\text{ref}}}^{\gamma-1}\right)^{-1}$ for the first and 1 for the remaining equations. Thereby, we can guarantee that the discrete asymptotic limit and the computed reference solution coincide.*

- *Since the solution of the limit method corresponds to the solution of the fully implicit discretization with the corresponding implicit Runge-Kutta method, the discretization is stable and therefore we can call our asymptotically consistent method* asymptotic preserving.

- *The proof of the asymptotic consistency does not rely on the fact that the equations are two-dimensional. In fact, the three-dimensional case is also covered.*

6.2. Asymptotic stability

We have analytically proven that the present method is asymptotically consistent. Thus, the method is suitable for solving problems in the low Mach regime. It remains to show that the method is also asymptotically stable. At this moment, we do not have a proof that the method is indeed asymptotically stable. (For preliminary work in this direction, we refer to the work of Zakerzadeh [23] and Zakerzadeh and Noelle [20].) Therefore, we investigate its stability based on numerics. More precisely, we consider the periodic wave example, given in Expl. 1, on a rectangular grid. For several values of $\Delta t/\Delta x = \text{CFL} \cdot \max \|\boldsymbol{u}^0\|$ and ε, we perform a fixed number of time iterations, in this case 100, for different total polynomial degrees. If the L^2 norm increases we state that the numerical method is unstable for this combination. Of course such a test can only be a rough indication of stability, and not replace a proof.

In Fig. 4 we summarized the results of this analysis. Note that the values $\Delta t/\Delta x$ also correspond to the advective CFL number, since the numerical example is chosen in such a way that $\max \|\boldsymbol{u}^0\| = 1$. For

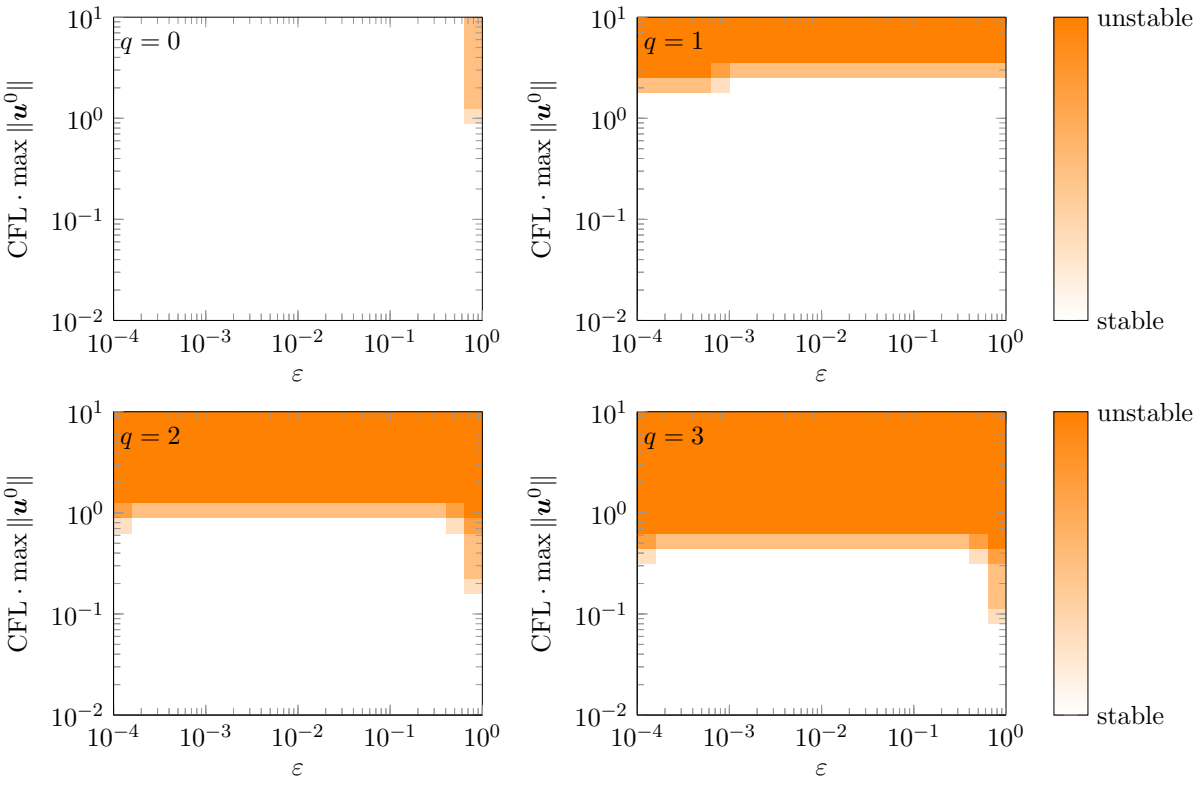

Figure 4: Stability analysis of the RS-IMEX DG method for $q = 0$ with the IMEX-Euler method (top, left), $q = 1$ with the IMEX-DPA-242 method (top,right), $q = 2$ with the IMEX-BPR-353 method (bottom,left) and $q = 3$ with the IMEX-ARK-4A2 method (bottom,right). In all cases a fixed grid was chosen, and 100 time-steps were performed. If the L^2 norm raises over a specific threshold we call the method unstable (orange) if it keeps below a specific threshold we call the method stable (white).

the low order ($q = 0$) case, one can see that stability is very pronounced. This is a result of the relatively large numerical diffusion in the numerical flux. For the higher order case the influence of the numerical flux function is much less pronounced. There is a threshold in the CFL number below which the method is stable. Fortunately, this threshold is independent of ε; it gets smaller with q increasing. (This is of course for standard DG known quite well [60].) Furthermore, we can observe that for larger ε, the method is only stable for less values of the CFL number. Because with $\varepsilon \to 0$, the influence of the implicit method gets more pronounced, this is to be expected.

Remark 10. *The given numerical results show that the numerical method is stable for a constant value of* $CFL \cdot \max \|\boldsymbol{u}^0\|$*, independently of* ε*. Therefore we call the method* asymptotically stable.

6.3. Asymptotic accuracy

In Sec. 2 we presented two different numerical examples where the exact solution is given, both essentially depending on a traveling vortex. Because of Subsec. 6.2 we know how to choose the relation $\mathrm{CFL} \cdot \max \|\boldsymbol{u}^0\|$ to obtain a stable numerical method. Since our goal is to compare all results and use a time-restriction which is also valid for large values of ε, we from now on take

$$\frac{\Delta t}{\Delta x} = \mathrm{CFL} \cdot \max \|\boldsymbol{u}^0\| = 0.05.$$

Grids have been generated with quadratic cells, the reference solution is always computed on the same grid as the forward solution with a fully implicit method. Results are compared using the L^1-norm of the error. Results are presented in the following.

6.3.1. Traveling vortex example

In Fig. 5, convergence of the first, second, third and fourth order ($q = 0, 1, 2, 3$) RS-IMEX DG method is plotted for different values of ε for the traveling vortex of Bispen, as given in Expl. 2. For the low order case we obtain the correct convergence order. For the first order case, it takes several refinements until the optimal order is reached. This is most likely due to the relatively large implicit stabilization. The reference solution for the second order case has a lower accuracy (though the correct convergence order) than the resulting compressible solution. This observation leads us to the conjecture that the reference solution is not needed to be computed as accurately as the compressible solution and therefore may be obtained on a coarser grid or with a lower polynomial degree; a fact that will certainly be exploited in future work.

For the high-order cases we see that the correct convergence order is not attained. This is not a surprise, because this example is not sufficiently smooth. For the fourth order method and for $\varepsilon = 10^{-4}$ the method stalls in converging. We assume that this is due to numerical roundoff errors that occur for high-order methods more frequently.

6.3.2. High-order example

In Fig. 6, convergence of the high-order vortex (Expl. 3) is shown for different values of ε and for different orders.

We can directly see that nearly all methods show their desired convergence order, just the case $q = 2$ shows a slightly strange behavior. First of all for $\varepsilon = 1$, the method seems to degrade to first order. This could be a result of the combination of methods or maybe a small instability since we have seen for the asymptotic stability that the case $\varepsilon = 1$ is the most unstable case. Furthermore, the convergence order of this formally third order method is only ≈ 2.7. Since all other methods deliver the desired results, we believe that this effect is not due to the low Mach number, but unsufficient grid resolution.

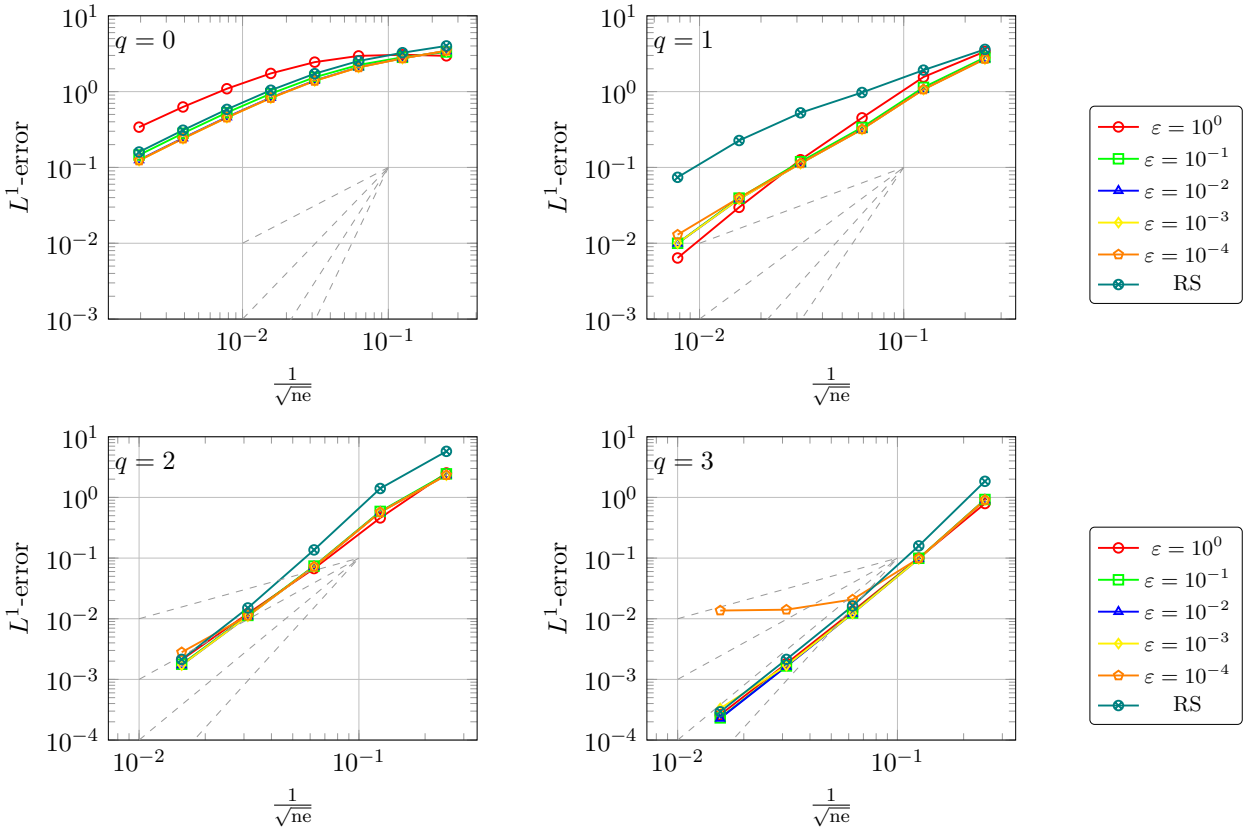

Figure 5: Convergence of the RS-IMEX DG method for traveling vortex: Different values of ε and for $q = 0$ with the IMEX-Euler method (top, left), $q = 1$ with the IMEX-DPA-242 method (top,right), $q = 2$ with the IMEX-BPR-353 method (bottom,left) and $q = 3$ with the IMEX-ARK-4A2 method (bottom,right). As an error measure, we chose the L^1 error between the numerical solution and the exact solution. The dashed lines give the different optimal convergence order, from first order up to fourth order.

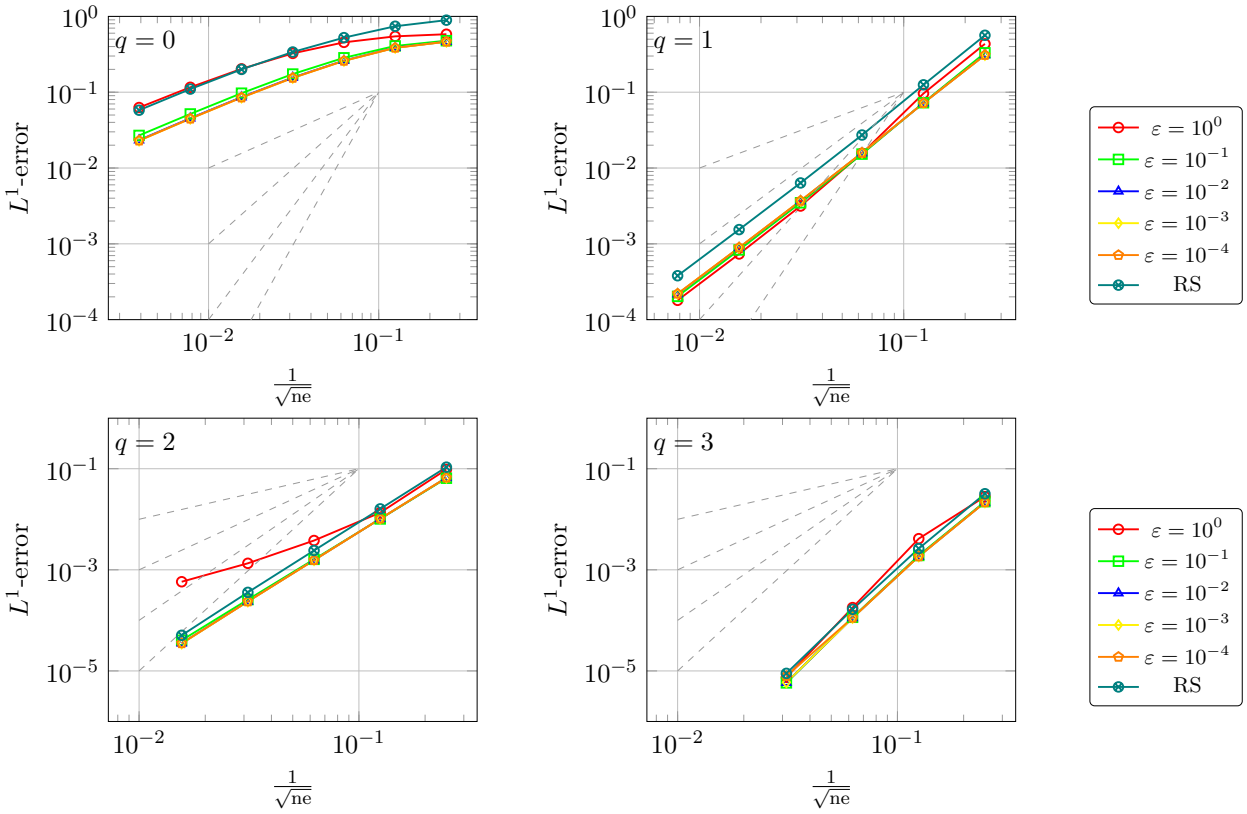

Figure 6: Convergence of the RS-IMEX DG method for high-order vortex: Different values of ε and for $q = 0$ with the IMEX-Euler method (top, left), $q = 1$ with the IMEX-DPA-242 method (top,right), $q = 2$ with the IMEX-BPR-353 method (bottom,left) and $q = 3$ with the IMEX-ARK-4A2 method (bottom,right). As an error measure, we chose the L^1 error between the numerical solution and the exact solution. The dashed lines give the different optimal convergence order, from first order up to fourth order.

Remark 11. *The numerical results show in some sense a biased behavior. While there seems to be no problem with stability, accuracy can get lost in special cases. What we have seen in the last numerical example, however, gives rise to the conjecture that the method is indeed* asymptotically accurate. *This remains under further investigation.*

Remark 12. *We have run similar tests for triangular elements. It seems that the shape of the element does not play a significant role.*

7. Conclusion and outlook

In the current paper we have coupled the RS-IMEX splitting with a high-order temporal and spatial discretization. The resulting method has been shown to be asymptotically consistent, and due to the structure of the limit method it has been shown that it is asymptotic preserving. Furthermore, numerical results give rise to the conjecture that the method is asymptotically stable and asymptotically accurate.

The next important steps in the development of the RS-IMEX splitting are inherent. First, a more detailed stability analysis is desirable to prove analytically that the method is stable under a convective CFL restriction. Second, the identification of more complex test-cases or equations is useful to test the method in a large range of settings.

Furthermore, reducing the computational effort is extremely important, especially compared to other numerical methods given in literature. Therefore our aim is to figure out in which way the reference solution can be computed the most efficiently, especially if a less accurate reference solution can also be employed. Another step is the usage of more efficient numerical methods for the implicit part, e.g., the hybridized discontinuous Galerkin method for spatial discretization (see e.g. [61, 62, 63, 64, 65]).

Finally, and this is somehow more of a long time goal, the identification of several high-order IMEX time integration methods is needed to obtain a numerical method of order larger than four.

8. Acknowledgment

The authors would like to thank Sebastian Noelle for fruitful discussions.

The first author has been partially supported by the German Research Foundation (DFG) project NO 361/3-3, and the University of Hasselt in the framework of the BOF 2016.

A. IMEX Runge-Kutta methods

For the sake of completeness, we list the employed Runge-Kutta methods in this appendix section. Note that for our setting, we only need the Butcher matrices $\widetilde{A}$ and $\widehat{A}$.

0	0	0	0
0	1	1	0

Table 2: A first order IMEX RK method called IMEX-Euler [27]. Left: implicit $\tilde{A}$, right: explicit $\hat{A}$.

References

[1] J. Schütz, K. Kaiser, A new stable splitting for singularly perturbed ODEs, Applied Numerical Mathematics 107 (2016) 18–33.

1/2	0	0	0	0	0	0	0
1/6	1/2	0	0	1/3	0	0	0
-1/2	1/2	1/2	0	1	0	0	0
3/2	-3/2	1/2	1/2	1/2	0	1/2	0

Table 3: A second order IMEX RK method called IMEX-DPA-242 [32]. Left: implicit $\tilde{A}$, right: explicit $\hat{A}$.

0	0	0	0	0	0	0	0	0	0
1/2	1/2	0	0	0	1	0	0	0	0
5/18	-1/9	1/2	0	0	4/9	2/9	0	0	0
1/2	0	0	1/2	0	1/4	0	3/4	0	0
1/4	0	3/4	-1/2	1/2	1/4	0	3/4	0	0

Table 4: A third order IMEX RK method called IMEX-BPR-353[28]. Left: implicit $\tilde{A}$, right: explicit $\hat{A}$.

[2] K. Kaiser, J. Schütz, R. Schöbel, S. Noelle, A new stable splitting for the isentropic Euler equations, IGPM Preprint Nr. 442 (2016).

[3] J. D. Anderson, Fundamentals of Aerodynamics, 3^{rd} Edition, McGraw-Hill New York, 2001.

[4] P. Wesseling, Principles of Computational Fluid Dynamics, Vol. 29 of Springer Series in Computational Mechanics, Springer Verlag, 2001.

[5] S. Klainerman, A. Majda, Singular limits of quasilinear hyperbolic systems with large parameters and the incompressible limit of compressible fluids, Communications on Pure and Applied Mathematics 34 (1981) 481–524.

[6] S. Schochet, Fast singular limits of hyperbolic PDEs, Journal of Differential Equations 114 (2) (1994) 476–512.

[7] W.-A. Yong, A note on the zero Mach number limit of compressible Euler equations, Proceedings of the American Mathematical Society 133 (10) (2005) 3079–3085.

[8] D. Kröner, Numerical Schemes for Conservation Laws, Wiley Teubner, 1997.

[9] G. Bispen, K. Arun, M. Lukáčová-Medvid'ová, S. Noelle, IMEX large time step finite volume methods for low Froude number shallow water flows, Communications in Computational Physics 16 (2014) 307–347.

[10] F. Cordier, P. Degond, A. Kumbaro, An asymptotic-preserving all-speed scheme for the Euler and Navier-Stokes equations, Journal of Computational Physics 231 (2012) 5685–5704.

0	0	0	0	0	0	0	0	0	0	0	0	0	0
-1/6	1/2	0	0	0	0	0	1/3	0	0	0	0	0	0
1/6	-1/3	1/2	0	0	0	0	1/6	1/6	0	0	0	0	0
3/8	-3/8	0	1/2	0	0	0	1/8	0	3/8	0	0	0	0
1/8	0	3/8	-1/2	1/2	0	0	1/8	0	3/8	0	0	0	0
-1/2	0	3	-3	1	1/2	0	1/2	0	-3/2	0	2	0	0
1/6	0	0	0	2/3	-1/2	2/3	1/6	0	0	0	2/3	1/6	0

Table 5: A fourth order IMEX RK method called IMEX-ARK-4A2[33]. Left: implicit $\tilde{A}$, right: explicit $\hat{A}$.

[11] P. Degond, M. Tang, All speed scheme for the low Mach number limit of the isentropic Euler equation, Communications in Computational Physics 10 (2011) 1–31.

[12] F. Giraldo, M. Restelli, M. Läuter, Semi-implicit formulations of the Navier-Stokes equations: Application to nonhydrostatic atmospheric modeling, SIAM Journal on Scientific Computing 32 (6) (2010) 3394–3425.

[13] J. Haack, S. Jin, J.-G. Liu, An all-speed asymptotic-preserving method for the isentropic Euler and Navier-Stokes equations, Communications in Computational Physics 12 (2012) 955–980.

[14] R. Klein, Semi-implicit extension of a Godunov-type scheme based on low Mach number asymptotics I: One-dimensional flow, Journal of Computational Physics 121 (1995) 213–237.

[15] A. Müller, J. Behrens, F. Giraldo, V. Wirth, Comparison between adaptive and uniform discontinuous Galerkin simulations in dry 2d bubble experiments, Journal of Computational Physics 235 (2013) 371–393.

[16] S. Noelle, G. Bispen, K. Arun, M. Lukáčová-Medvid'ová, C.-D. Munz, A weakly asymptotic preserving low Mach number scheme for the Euler equations of gas dynamics, SIAM Journal on Scientific Computing 36 (2014) B989–B1024.

[17] M. Restelli, Semi-lagrangian and semi-implicit discontinuous Galerkin methods for atmospheric modeling applications, PhD thesis Politecnico di Milano.

[18] L. Yelash, A. Müller, M. Lukáčová-Medvid'ová, F. X. Giraldo, V. Wirth, Adaptive discontinuous evolution Galerkin method for dry atmospheric flow, Journal of Computational Physics 268 (2014) 106–133.

[19] J. Schütz, S. Noelle, Flux splitting for stiff equations: A notion on stability, Journal of Scientific Computing 64 (2) (2015) 522–540.

[20] H. Zakerzadeh, S. Noelle, A note on the stability of implicit-explicit flux splittings for stiff hyperbolic systems, IGPM Preprint Nr. 449 (2016).

[21] F. X. Giraldo, M. Restelli, High-order semi-implicit time-integrators for a triangular discontinuous Galerkin oceanic shallow water model, International Journal for Numerical Methods in Fluids 63 (9) (2010) 1077–1102.

[22] F. Filbet, S. Jin, A class of asymptotic-preserving schemes for kinetic equations and related problems with stiff sources, Journal of Computational Physics 229 (20) (2010) 7625–7648.

[23] H. Zakerzadeh, Asymptotic analysis of the RS-IMEX scheme for the shallow water equations in one space dimension, IGPM Preprint Nr. 455 (2016).

[24] U. M. Ascher, S. Ruuth, B. Wetton, Implicit-Explicit methods for time-dependent partial differential equations, SIAM Journal on Numerical Analysis 32 (1995) 797–823.

[25] W. Hundsdorfer, J. Jaffré, Implicit–explicit time stepping with spatial discontinuous finite elements, Applied Numerical Mathematics 45 (2) (2003) 231–254.

[26] W. Hundsdorfer, S.-J. Ruuth, IMEX extensions of linear multistep methods with general monotonicity and boundedness properties, Journal of Computational Physics 225 (2) (2007) 2016–2042.

[27] U. M. Ascher, S. Ruuth, R. Spiteri, Implicit-explicit Runge-Kutta methods for time-dependent partial differential equations, Applied Numerical Mathematics 25 (1997) 151–167.

[28] S. Boscarino, L. Pareschi, G. Russo, Implicit-explicit Runge–Kutta schemes for hyperbolic systems and kinetic equations in the diffusion limit, SIAM Journal on Scientific Computing 35 (1) (2013) A22–A51.

[29] C. A. Kennedy, M. H. Carpenter, Additive Runge-Kutta schemes for convection-diffusion-reaction equations, Applied Numerical Mathematics 44 (2003) 139–181.

[30] L. Pareschi, G. Russo, Implicit-explicit Runge-Kutta schemes for stiff systems of differential equations, Recent Trends in Numerical Analysis 3 (2000) 269–289.

[31] G. Russo, S. Boscarino, IMEX Runge-Kutta schemes for hyperbolic systems with diffusive relaxation, European Congress on Computational Methods in Applied Sciences and Engineering (ECCOMAS 2012).

[32] G. Dimarco, L. Pareschi, Asymptotic preserving implicit-explicit Runge–Kutta methods for nonlinear kinetic equations, SIAM Journal on Numerical Analysis 51 (2) (2013) 1064–1087.

[33] H. Liu, J. Zou, Some new additive Runge–Kutta methods and their applications, Journal of Computational and Applied Mathematics 190 (1-2) (2006) 74–98.

[34] B. Cockburn, S. Hou, C.-W. Shu, The Runge–Kutta local projection discontinuous Galerkin finite element method for conservation laws IV: The multidimensional case, Mathematics of Computation 54 (1990) 545–581.

[35] B. Cockburn, S. Y. Lin, C.-W. Shu, TVB Runge-Kutta local projection discontinuous Galerkin finite element method for conservation laws III: One dimensional systems, Journal of Computational Physics 84 (1989) 90–113.

[36] B. Cockburn, C.-W. Shu, TVB Runge-Kutta local projection discontinuous Galerkin finite element method for conservation laws II: General framework, Mathematics of Computation 52 (1988) 411–435.

[37] B. Cockburn, C.-W. Shu, The Runge-Kutta local projection p^1-discontinuous Galerkin finite element method for scalar conservation laws, RAIRO Mathematical modelling and numerical analysis 25 (1991) 337–361.

[38] B. Cockburn, C.-W. Shu, The Runge-Kutta discontinuous Galerkin Method for conservation laws V: Multidimensional Systems, Mathematics of Computation 141 (1998) 199–224.

[39] A. Kanevsky, M. H. Carpenter, D. Gottlieb, J. S. Hesthaven, Application of implicit-explicit high order Runge-Kutta methods to discontinuous-Galerkin schemes, Journal of Computational Physics 225 (2) (2007) 1753–1781.

[40] P.-O. Persson, High-order LES simulations using implicit-explicit Runge-Kutta schemes, AIAA Paper 11-684 (2011).

[41] H. Wang, C.-W. Shu, Q. Zhang, Stability and error estimates of local discontinuous Galerkin methods with implicit-explicit time-marching for advection-diffusion problems, SIAM Journal on Numerical Analysis 53 (1) (2015) 206–227.

[42] P. Degond, S. Jin, J.-G. Liu, Mach-number uniform asymptotic-preserving gauge schemes for compressible flows, Bulletin-Institute of Mathematics Academia Sinica (New Series) 2 (4) (2007) 851–892.

[43] S. Jin, Efficient asymptotic-preserving (AP) schemes for some multiscale kinetic equations, SIAM Journal on Scientific Computing 21 (1999) 441–454.

[44] S. Jin, Asymptotic preserving (AP) schemes for multiscale kinetic and hyperbolic equations: A review, Rivista di Matematica della Universita Parma 3 (2012) 177–216.

[45] G. Dimarco, L. Pareschi, Exponential Runge-Kutta methods for stiff kinetic equations, SIAM Journal on Numerical Analysis 49 (5) (2011) 2057–2077.

[46] G. Dimarco, L. Mieussens, V. Rispoli, An asymptotic preserving automatic domain decomposition method for the Vlasov-Poisson-BGK system with applications to plasmas, Journal of Computational Physics 274 (2014) 122–139.

[47] M. Ricchiuto, A. Bollermann, Stabilized residual distribution for shallow water simulations, Journal of Computational Physics 228(4) (4) (2009) 1071–1115.

[48] B. Schling, The Boost C++ Libraries, XML Press, 2011.

[49] BOOST C++ Libraries, `http://www.boost.org`.

[50] E. Hairer, G. Wanner, Solving Ordinary Differential Equations II, Springer Series in Computational Mathematics, 1991.

[51] S. Boscarino, Error analysis of IMEX Runge-Kutta methods derived from differential-algebraic systems, SIAM Journal on Numerical Analysis 45 (2007) 1600–1621.

[52] Y. Liu, M. Vinokur, Z. J. Wang, Discontinuous spectral difference method for conservation laws on unstructured grids, in: Proceedings of the 3rd International Conference on Computational Fluid Dynamics, July 12-16, 2004, Toronto, Canada, Springer, 2004.

[53] Y. Liu, M. Vinokur, Z. J. Wang, Spectral Difference method for unstructured grids I: Basic formulation, Journal of Computational Physics 216 (2) (2006) 780–801.

[54] Z. J. Wang, L. Zhang, Y. Liu., High-order spectral volume method for 2D Euler equations, AIAA Paper 03-3534 (2003).

[55] V. V. Rusanov, Calculation of interaction of non-steady shock waves with obstacles, NRC, Division of Mechanical Engineering.

[56] D. D. Pietro, A. Ern, Mathematical aspects of discontinuous Galerkin Methods, Vol. 69, Springer Science & Business Media, 2011.

[57] H. Guillard, C. Viozat, On the behavior of upwind schemes in the low Mach number limit, Computers and Fluids 28 (1) (1999) 63–86.

[58] E. Turkel, Preconditioned methods for solving the incompressible and low speed compressible equations, Journal of Computational Physics 72 (2) (1987) 277 – 298.

[59] G. Bispen, IMEX finite volume methods for the shallow water equations, Ph.D. thesis, Johannes Gutenberg-Universität (2015).

[60] B. Cockburn, C. W. Shu, Runge-Kutta discontinuous Galerkin methods for convection-dominated problems, Journal of Scientific Computing 16 (2001) 173–261.

[61] N. Nguyen, J. Peraire, B. Cockburn, A hybridizable discontinuous Galerkin method for the incompressible navier-stokes equations, AIAA Paper 2010-362.

[62] J. Peraire, N. C. Nguyen, B. Cockburn, A hybridizable discontinuous Galerkin method for the compressible Euler and Navier-Stokes equations, AIAA Paper 10-363 (2010).

[63] A. Jaust, J. Schütz, M. Woopen, An HDG method for unsteady compressible flows, in: R. M. Kirby, M. Berzins, J. S. Hesthaven (Eds.), Spectral and High Order Methods for Partial Differential Equations ICOSAHOM 2014, Vol. 106 of Lecture Notes in Computational Science and Engineering, Springer International Publishing, 2015, pp. 267–274.

[64] A. Jaust, J. Schütz, M. Woopen, A hybridized discontinuous Galerkin method for unsteady flows with shock-capturing, AIAA Paper 2014-2781.

[65] J. Schütz, M. Woopen, G. May, A hybridized DG/mixed scheme for nonlinear advection-diffusion systems, including the compressible Navier-Stokes equations, AIAA Paper 2012-0729.

universiteit hasselt

UHasselt Computational Mathematics Preprint Series

UP-16-01 *Jochen Schütz and Vadym Aizinger*, **A hierarchical scale separation approach for the hybridized discontinuous Galerkin method**, 2016

UP-16-02 *Klaus Kaiser, Jochen Schütz, Ruth Schöbel and Sebastian Noelle*, **A new stable splitting for the isentropic Euler equations**, 2016

UP-16-03 *Sergey Alyaev, Eirik Keilegavlen, Jan Martin Nordbotten, Iuliu Sorin Pop*, **Fractal structures in freezing brine**, 2016

UP-16-04 *Florin A. Radu, Kundan Kumar, Jan Martin Nordbotten, Iuliu Sorin Pop*, **A robust, mass conservative scheme for two-phase flow in porous media including Hölder continuous nonlinearities**, 2016

UP-16-05 *Stefan Karpinski, Iuliu Sorin Pop, Florin A. Radu*, **Analysis of a linearization scheme for an interior penalty discontinuous Galerkin method for two phase flow in porous media with dynamic capillarity effects**, 2016

UP-16-06 *Klaus Kaiser and Jochen Schütz*, **A high-order method for weakly compressible flows**, 2016

All rights reserved.